Supporting Information for 'LEGO Bricks-Inspired Ultra-Stable and Rapid Transport 2D Membrane for Fast Water Purification'

Bo Zhu[a], Nan Li[b*], Changsheng Guo[c], Pengbi Liu[c], Tianyu Li[a], Lijing Wang[a], Zhiwei Xu[a*]

[a] State Key Laboratory of Separation Membranes and Membrane Processes, School of Textile Science and Engineering, Tiangong University, Tianjin 300387, China

[b] State Key Laboratory of Separation Membranes and Membrane Processes, School of Chemistry, Tiangong University, Tianjin 300387, China

[c] School of Textile Materials and Engineering, Wuyi University, Jiangmen 529020, China

Functionalized graphene oxide (GO) nanosheets

In brief, particle-size homogenised GO nanosheets (50 mg) were sonicated to achieve uniform dispersion in 10 mL of deionized water, with the pH adjusted to 7.2 using PBS solution. Subsequently, a precise quantity of EDC/NHS (1.15 mmol, molar ratio of 1:1) was added for activation, and the mixture was allowed to react for 1 hour. Following this, amantadine hydrochloride (50 mg) was introduced to the dispersion and completely dissolved. The reaction was then stirred continuously at 40°C for 24 hours. Finally, the reaction product was subjected to centrifugation, the supernatant was discarded, and the resulting powder underwent repeated centrifugation with deionized water at least 5 times, before being freeze-dried to yield the fGO powder.

Grazing-in Wide-angle X-ray Scattering

A grazing-in wide-angle X-ray scattering experiment on membranes was executed at the BL16B1 beamline at the Shanghai Synchrotron Radiation Facility in China. The tests were performed in the mode of incident X-rays along the direction of the membrane cross-section to obtain the stacking information of the nanosheets. In order to quantitatively describe the state of nanosheet stacking, an orientation distribution coefficient S based on Hermans is introduced here for directly evaluating the orientation information of nanosheets.[1-3] The value of S is in the interval of -0.5 to 1. When S=1 and -0.5 indicate that the nanosheets are perfectly oriented along the directions of θ=0° and θ=90°, respectively, whereas S=0 indicates that the nanosheet stacking is anisotropic. The S can be calculated according to the following equation:[2]

$$S = \frac{1}{2}\left(3\langle cos^2\theta\rangle - 1\right) \quad \text{S1}$$

where $\langle cos^2\theta\rangle$ represents the average cosine-squared weighted azimuthal intensity I(θ), which can be calculated by the following formula:

$$\langle cos^2\theta\rangle = \frac{\int_0^{2\pi} I(\theta) cos^2\theta \sin\theta d\theta}{\int_0^{2\pi} I(\theta)\sin\theta d\theta} \quad \text{S2}$$

GIWAXS-Tools and Nika package are used to reduce the two-dimensional scattering pattern to one-dimensional scattering curve and do the corresponding data processing. (Jianyao Huang, GIWAXS-Tools, Version (2.1.6), https://gitee.com/swordshinehjy/giwaxs-script (accessed on 23rd November 2023)

Membrane Performance Assessment

Membrane permeance P and rejection R are calculated according to the following

formula respectively:[4]

$$P = \frac{V}{A\Delta t\Delta p} \quad \text{S3}$$

$$R = \frac{C_f - C_P}{C_f} \quad \text{S4}$$

where V denotes the volume of permeate (L), A represents the effective area of membrane filtration (cm^2), Δt is the collection time of permeate (h), and Δp is the transmembrane pressure difference during filtration. C_f and C_P are the solution concentrations of permeate and feed solution, respectively.

The separation factor *S* of the dye and salt was calculated using the following equation:[5]

$$S = \frac{1 - R_{salt}}{1 - R_{dye}} \quad \text{S5}$$

where R_{salt} and R_{dye} refer to the salt and dye retention rates of the membrane, respectively.

Nanoindentation Experiment

The pressure resistance of membranes was evaluated using nanoindentation technique. The hardness of nanoindentation is defined as the ratio of the indentation load to the projected contact area of the indentation. It is the average pressure that a material can withstand under load. According to the load-displacement curve, the hardness H under peak load can be calculated by the equation S6:[6]

$$H = \frac{P_{max}}{A} \quad \text{S6}$$

where A represents the indentation projected contact area and P_{max} represents is the maximum indentation load. The Berkovich probe used in this study has a projected

contact area as a function of contact depth. A series of indentation tests were performed on the membrane surface in a 2×2 point array with load control for all loading points. To avoid disturbances between indentation points, each point was spaced 5 to 10 times the indentation contact depth. To ensure the accuracy of the data, the indentation load was 200 μN and the indentation point spacing was 2 μm.

Molecular Dynamics Simulation

In this study, three GO nanosheet models with different particle sizes were first constructed by using the Material Visualize module based on the Material Studio (MS) software package, as shown in Figure S10. Aiming to approximate the distribution of oxygen-containing functional groups in the actual GO nanosheets, the degree of oxidation (C/O ratio) and the percentage of oxygen-containing functional groups in each GO nanosheet model were determined based on the XPS elemental analysis (Table S1) and randomly distributed on both sides of the graphene. The GO nanosheets were also grafted with amantadine to obtain fGO nanosheet molecular structure models based on the elemental analysis of fGO (Figure S11). In addition, the compound structure model of HA-CD was constructed using MS and randomly assembled into the interlayers of fGO nanosheets to obtain the HA-CD@fGOm model (Figure S13). It is worth mentioning that the spacing of the specific nanosheets was set and fixed according to the layer spacing of the membrane measured in the experiment (Table S2). To balance the flexible effect of GO membranes on water and ion migration, the oxygen-containing groups of GO nanosheets in the membrane models were free to move. The structural modeling nomenclature of all membranes is consistent with the

experiments. In the initial state, 0.5 mol•L^{-1} of Congo-red solution simulated the feed solution on the feed side, and pure water was added in the right osmotic side to balance the pressure difference between the left and right sides. Furthermore, due to the three-dimensional periodic boundaries, two reflective graphene sheets were placed on the right side of the right-side reservoir and on the left side of the left-side reservoir to prevent the solution from migrating from the boundary of one reservoir to the boundary of the other reservoir. A certain pressure was applied on the left graphene sheet while the right graphene sheet was kept fixed to simulate the transmembrane pressure difference of actual water molecules.

The SPC/E model was used to describe the solvent water molecule.[7] Lennard-Jones (LJ) parameters for other atoms and ions were taken from the Universal force field. LJ potentials were used to characterize the non-bonding interactions between particles. The particle-particle and particle-lattice methods (PPPM) were used to calculate the long-range electrostatic interaction forces with a cutoff value of 12 Å. The cutoff value for the calculation of the short-range interactions was 10 Å. All simulations were carried out using the Forcite module of MS software. The structure of each model was optimized under a Smart algorithm to achieve the minimum energy. The initial velocity of the system was randomized in the NVT system and the system temperature was stabilized at 300 K using a Nose-Hoover thermostat.After that, molecular dynamics simulations were executed for a period of 2000 ps with a time step of 0.5 fs.The water permeability of the interlayer channel is evaluated by the following equation S7: [8]

$$P_w = \frac{t \times N_w}{N_{w,p}} \tag{S7}$$

Where N_w is the total number of water molecules, t is the time, and $N_{w,p}$ is the number of water molecules on the feed side.

The diffusion coefficient of water molecules within the membrane is calculated by the equation S8: [9, 10]

$$D = \frac{1}{6}\lim_{n\to\infty}\frac{d}{dt}\sum_{i=1}^{N_a}\left\langle (r_i(t) - r_i(0))^2 \right\rangle \quad \text{(S8)}$$

where N_a is the number of diffusing atoms a, $\left\langle (r_i(t) - r_i(0))^2 \right\rangle$ is the mean square displacement (MSD) of the atom $r_i(t)$ and $r_i(0)$ denote the position vector of atom i at the time t and the initial time 0.

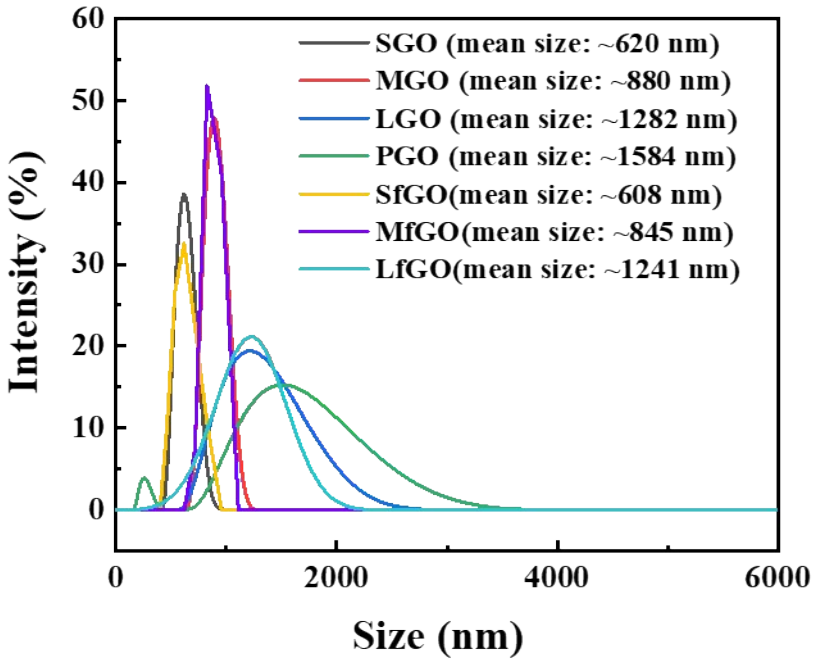

Figure S1. Particle size distribution of GO and fGO nanosheets.

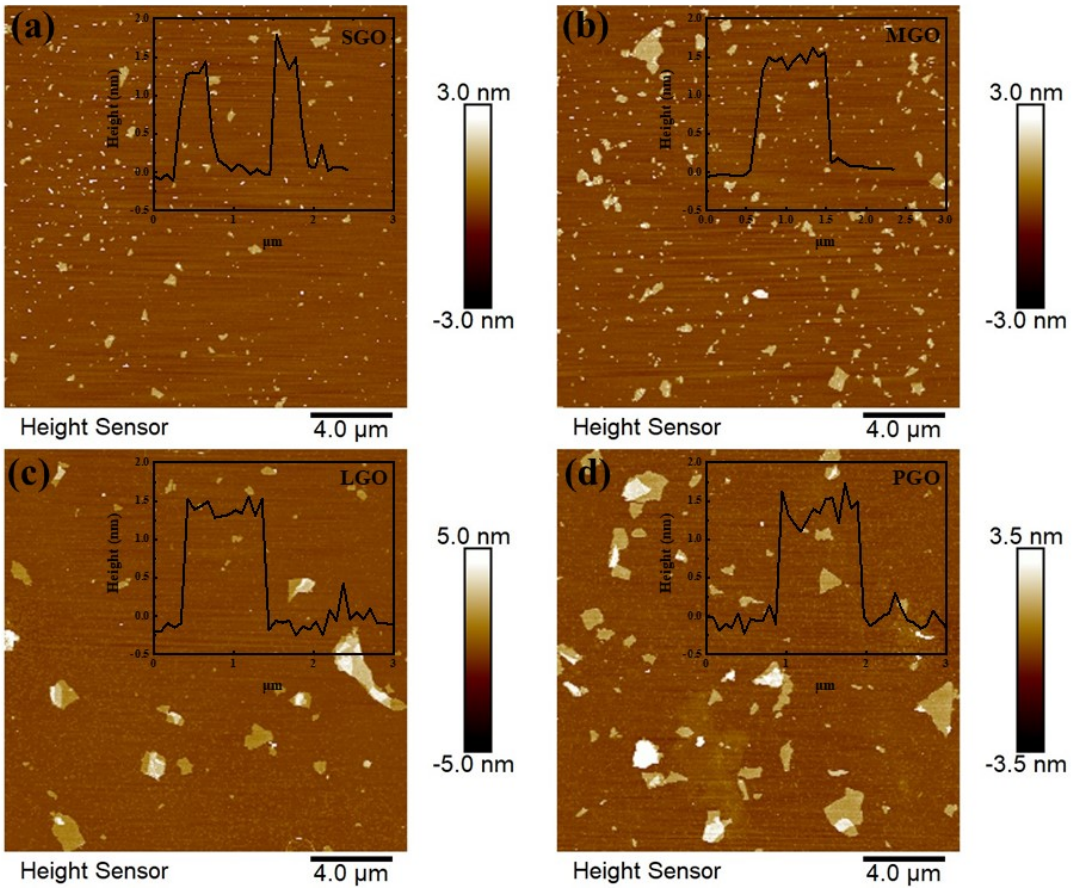

Figure S2. AFM characterization of ultrasonically exfoliated GO nanosheets.

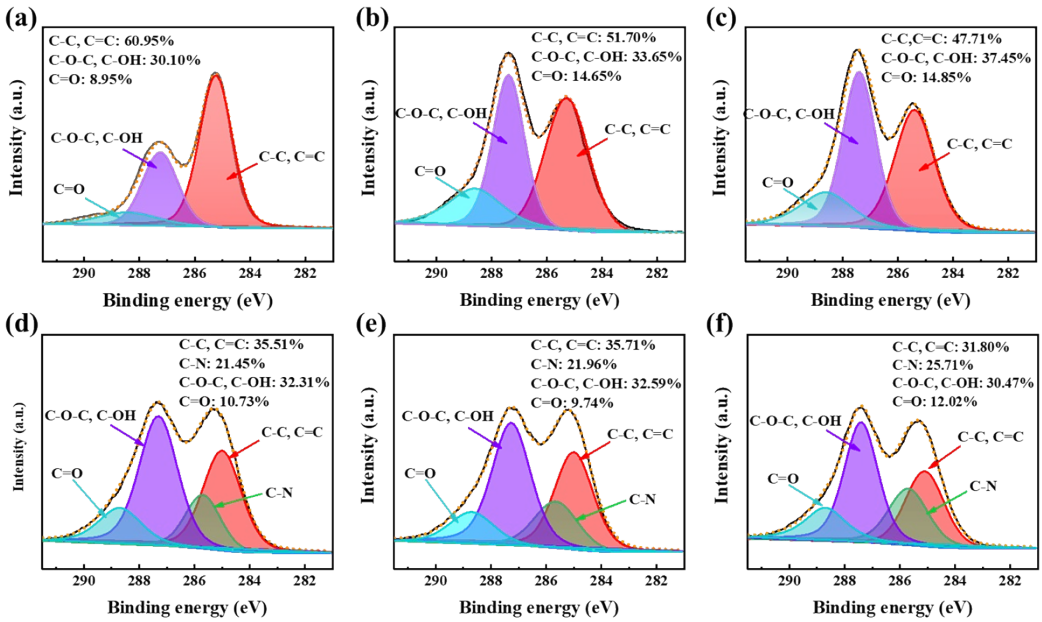

Figure S3. XPS C1s spectrum analysis of nanosheets: (a) LGO nanosheets, (b) MGO nanosheets, (c) SGO nanosheets, (d) LfGO nanosheets, (e) MfGO nanosheets, (f) SfGO nanosheets.

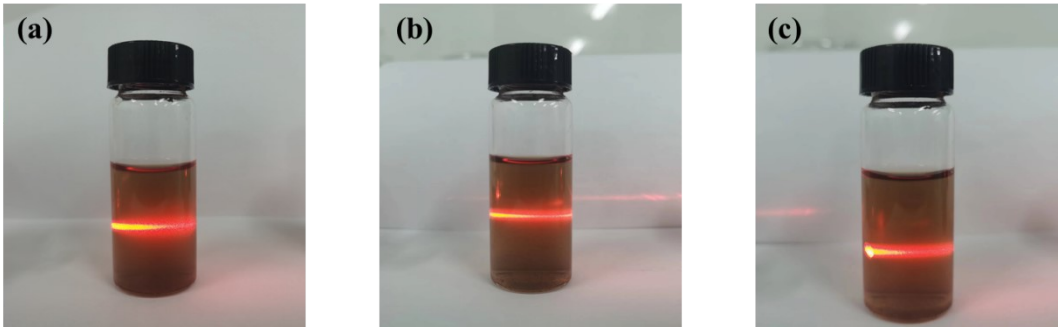

Figure S4. Digital photographs of laser irradiation after addition of HA-CD to fGO dispersions: (a) LfGO dispersion, (b) MfGO dispersion, (c) SfGO dispersion.

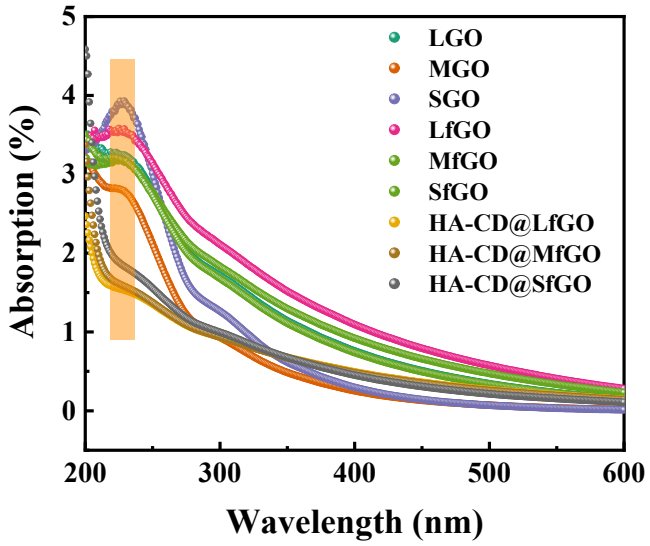

Figure S5. UV-Vis spectrum analysis of fGO dispersion after addition of HA-CD.

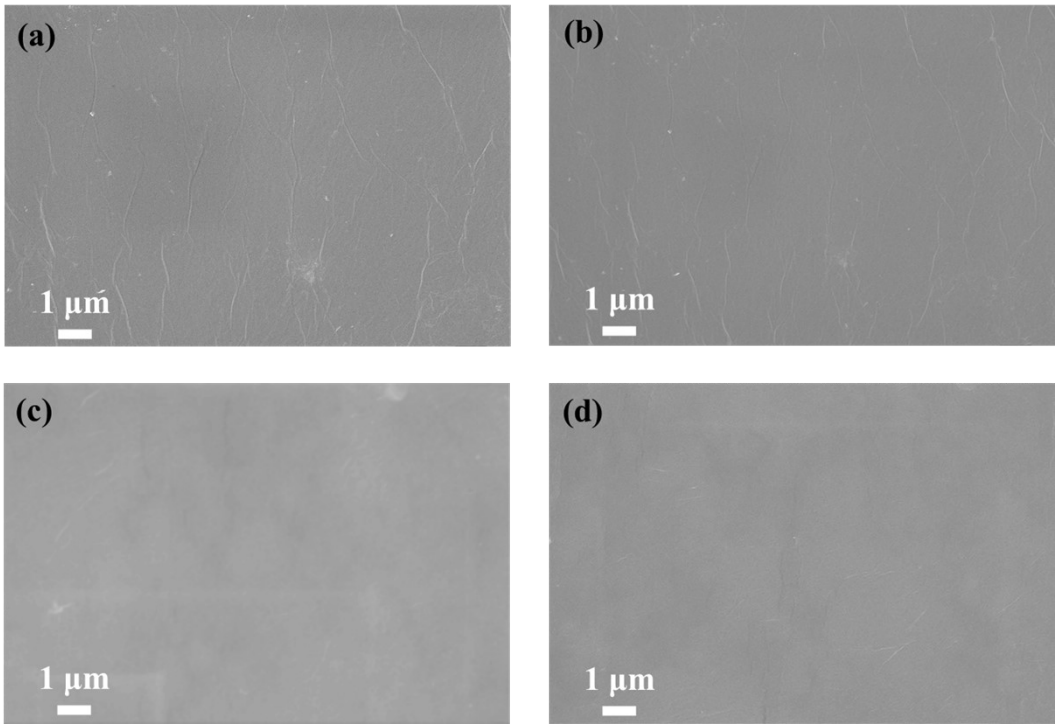

Figure S6. SEM image of the top surface of (a) LGOm, (b) MGOm, (c) HA-CD@LfGOm and (d) HA-CD@MfGOm.

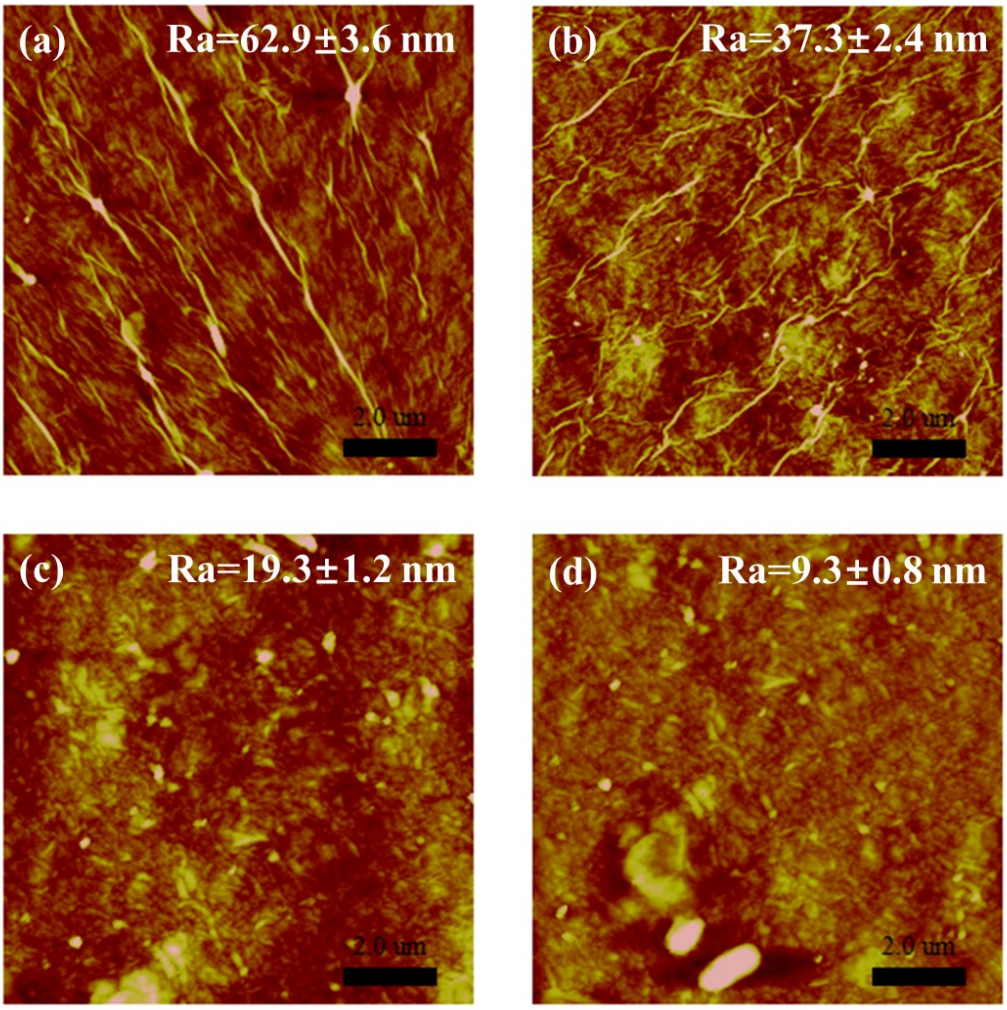

Figure S7. AFM image of (a) LGOm, (b) MGOm, (c) HA-CD@LfGOm and (d) HA-CD@MfGOm.

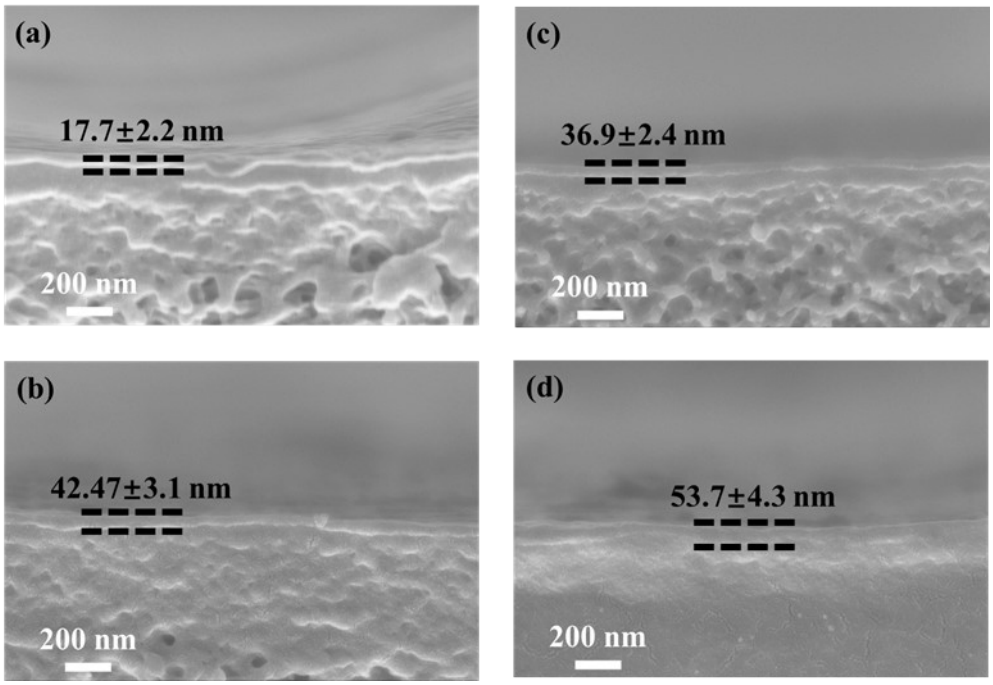

Figure S8. SEM image of the cross-section of HA-CD@SfGOm at different volume loading: (a) 10 mL, (b) 14 mL, (c) 17 mL and (d) 20 mL.

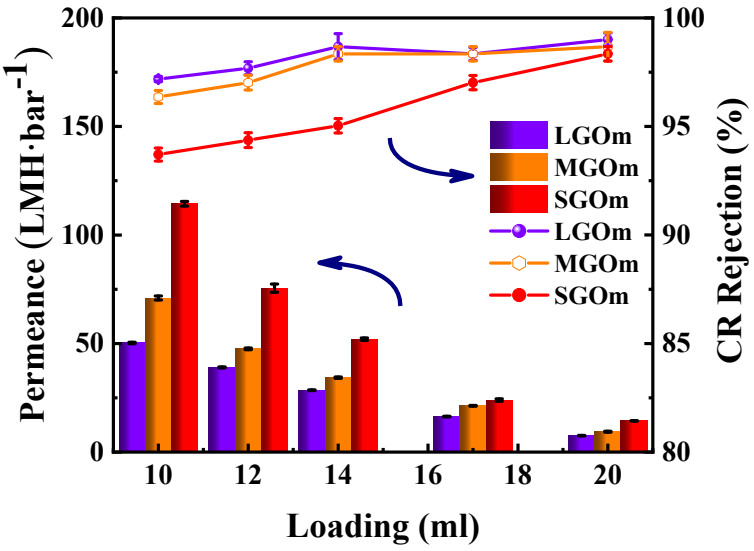

Figure S9. Effect of loading on the nanofiltration performance of GOm.

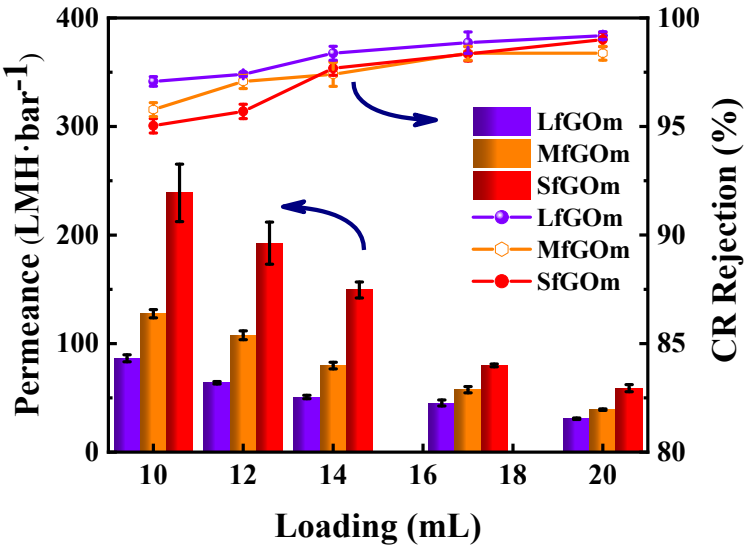

Figure S10. Effect of loading on the nanofiltration performance of fGOm.

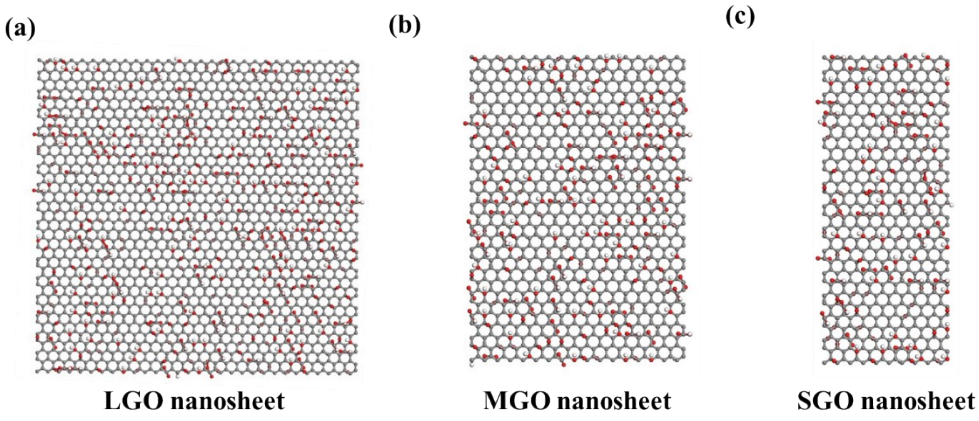

Figure S11. GO nanosheet structural models: (a) 30×30 Å, (b) 21×29.4 Å and (c) 11.5×29.4 Å.

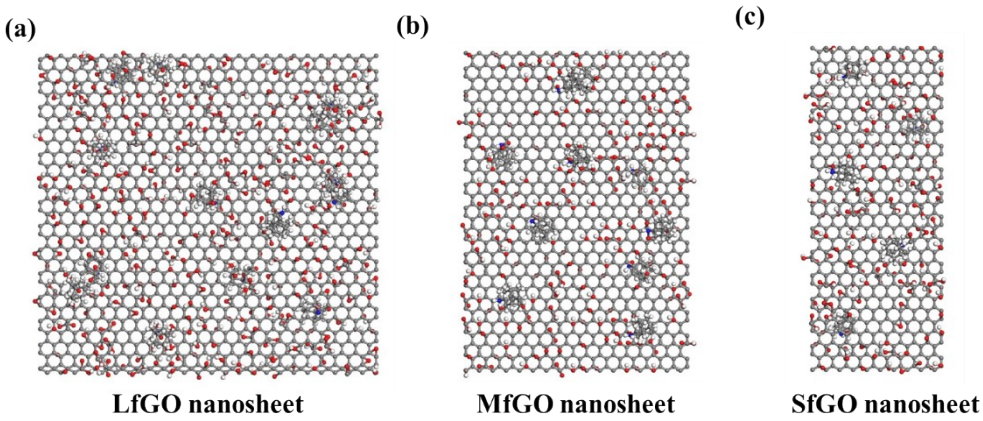

Figure S12. fGO nanosheet structural models: (a) 30×30 Å, (b) 21×29.4 Å and (c)

11.5×29.4 Å.

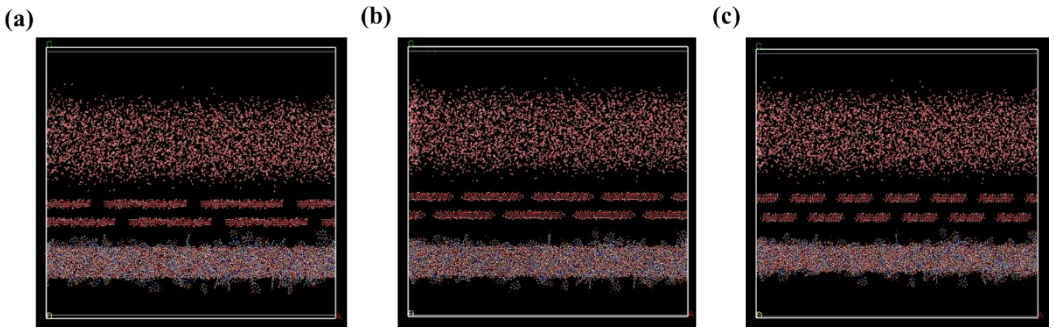

Figure S13. Initial mass transfer model box for (a) LGOm, (b) MGOm, and (c) SGOm.

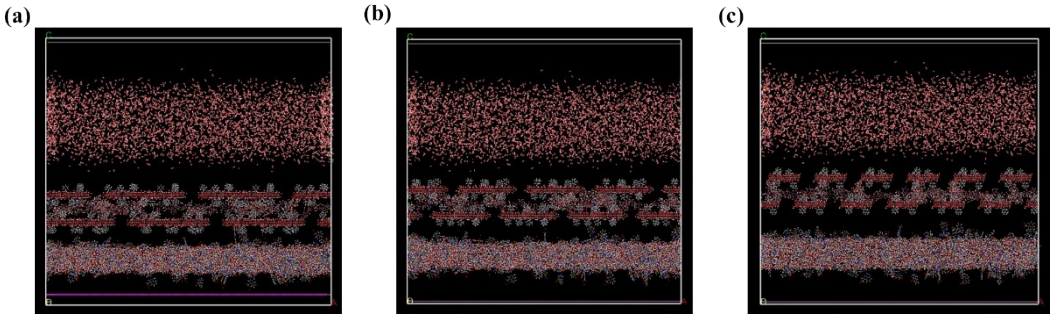

Figure S14. Initial mass transfer model box for (a) HA-CD@LfGOm, (b) HA-CD@MfGOm, and (c) HA-CD@SfGOm.

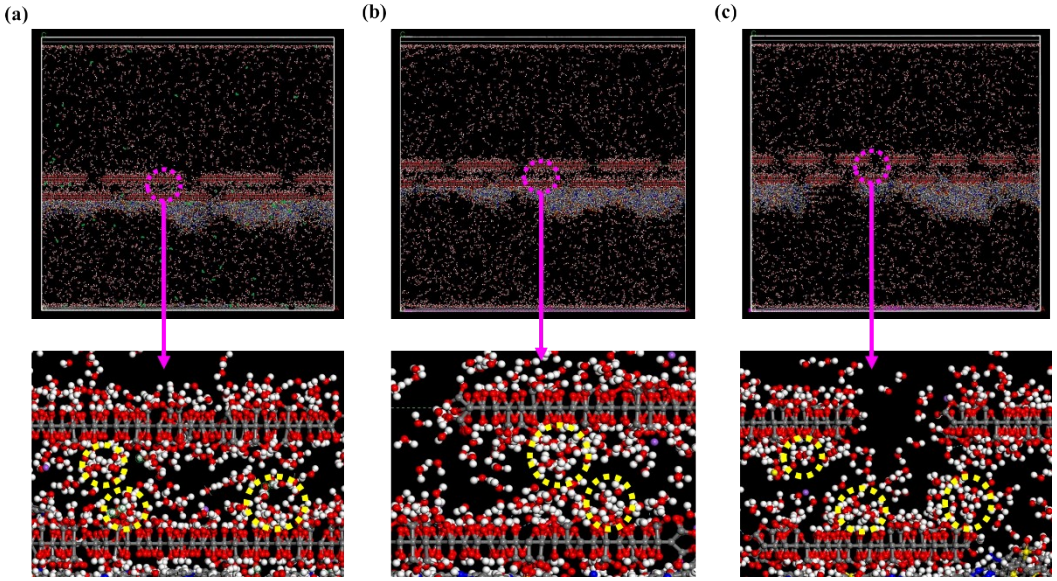

Figure S15. The 2 ns relaxation post mass transfer model box for (a) LGOm, (b) MGOm, and (c) SGOm. The structures circled in yellow are water molecule clusters.

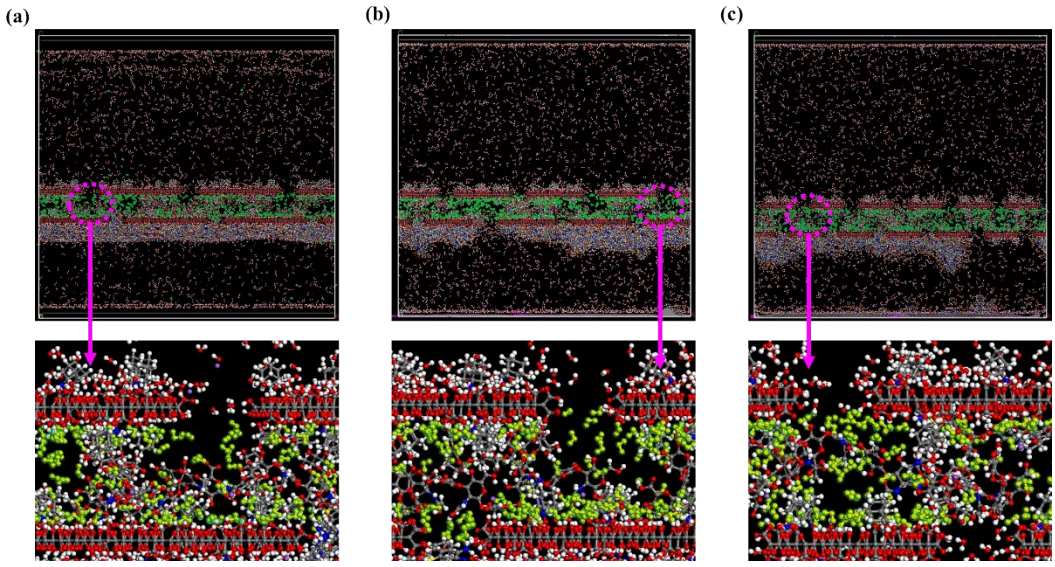

Figure S16. The 2 ns relaxation post mass transfer model box for (a) HA-CD@LfGOm, (b) HA-CD@MfGOm, and (c) HA-CD@SfGOm. The water molecules were marked in yellow.

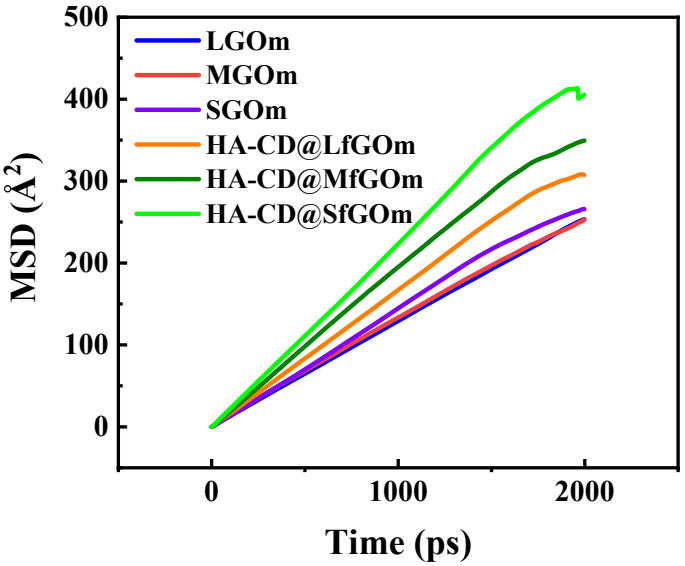

Figure S17. MSD of water molecules in the interlayer channel of LGOm, MGOm, SGOm, HA-CD@LfGOm, HA-CD@MfGOm, and HA-CD@SfGOm.

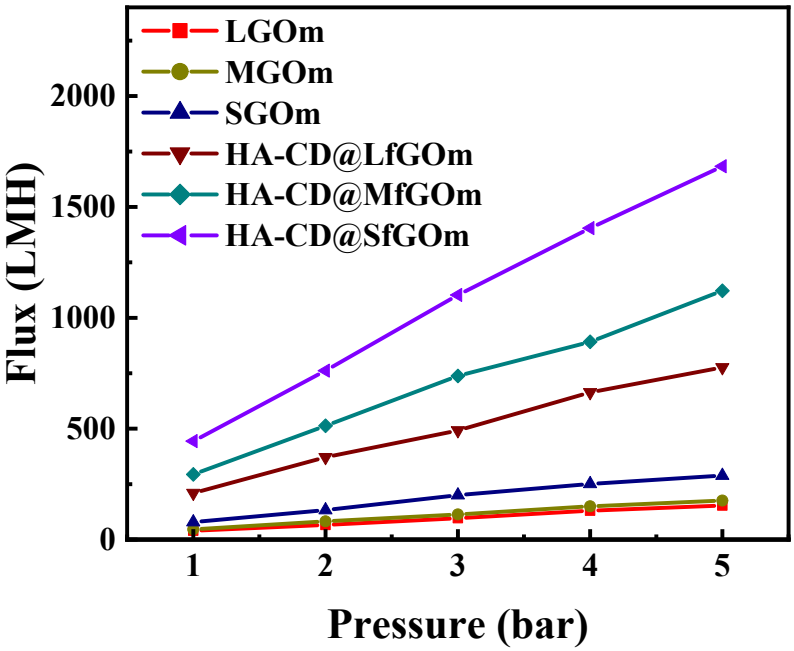

Figure S18. Effect of pressure change on membrane stability.

Table S1. Distribution of elemental content of nanosheets.

Atom	C (%)	N (%)	O (%)
LGO	69.2	0	30.8
MGO	66.47	0	33.53
SGO	62.03	0	37.97
LfGO	68.24	2.74	29.03
MfGO	66.96	3.63	29.41
SfGO	66.93	3.95	29.12

Table S2. Variation of layer spacing between dry and fully wetted states of the membrane.

d-spacing	Dried (nm)	Wet (nm)

LGOm	0.8	1.34
MGOm	0.84	1.36
SGOm	0.85	1.44
LfGOm	0.88	1.35
MfGOm	0.88	1.36
SfGOm	0.88	1.42
HA-CD@ LfGOm	1.93	1.95
HA-CD@ MfGOm	1.93	1.95
HA-CD@ SfGOm	1.96	1.98

References

(1) Hermans, J. J.; Hermans, P. H.; Vermaas, D.; Weidinger, A. Quantitative evaluation of orientation in cellulose fibres from the X-ray fibre diagram. *Recueil des Travaux Chimiques des Pays-Bas* **1946**, *65* (6), 427-447.

(2) Cao, Y.; Xiong, Z.; Xia, F.; Franks, G. V.; Zu, L.; Wang, X.; Hora, Y.; Mudie, S.; He, Z.; Qu, L.; et al. New Structural Insights into Densely Assembled Reduced Graphene Oxide Membranes. *Advanced Functional Materials* **2022**, *32* (42), 2201535.

(3) Zhang, Y.; Wang, S.; Tang, P.; Zhao, Z.; Xu, Z.; Yu, Z.-Z.; Zhang, H.-B. Realizing Spontaneously Regular Stacking of Pristine Graphene Oxide by a Chemical-Structure-Engineering Strategy for Mechanically Strong Macroscopic Films. *ACS Nano* **2022**, *16* (6), 8869-8880.

(4) Zhu, B.; Shao, R.; Li, N.; Guo, C.; Liu, P.; Shi, J.; Min, C.; Liu, S.; Qian, X.; Wang, L.; et al. Narrowing the pore size distribution of polyamide nanofiltration membranes via dragging piperazines to enhance ion selectivity. *Journal of Membrane Science* **2023**,

667, 121187.

(5) Han, Y.; Guo, C.; Liu, P.; Li, N.; Min, C.; Zhu, B.; Shi, H.; Pei, X.; Xu, Z. Graphene oxide membranes with short-range pore channels toward ultrafast water transport via γ-ray etching. *Applied Surface Science* **2023**, *608*, 155150.

(6) Xiaodong, L.; Hongsheng, G.; Wally, A. S.; Dongling, F.; Xiaoyou, X.; Michael, A. S.; Anthony, P. R.; Michael, L. M. Nanomechanical characterization of single-walled carbon nanotube reinforced epoxy composites. *Nanotechnology* **2004**, *15* (11), 1416.

(7) Berendsen, H. J. C.; Grigera, J. R.; Straatsma, T. P. The missing term in effective pair potentials. *The Journal of Physical Chemistry* **1987**, *91* (24), 6269-6271.

(8) Wu, J.; Li, N.; Liu, S.; Shi, W.; Min, C.; Zhu, B.; Shao, R.; Pei, X.; Cai, Z.; Xu, Z. Graphene oxide membranes with a confined mass transfer effect for Li+/Mg2+ separation: a molecular dynamics study. *Physical Chemistry Chemical Physics* **2022**, *24* (42), 26011-26022, 10.1039/D2CP03542A.

(9) Zhu, B.; Shao, R.; Li, N.; Guo, C.; Liu, P.; Shi, J.; Min, C.; Liu, S.; Qian, X.; Wang, L.; et al. Narrowing the pore size distribution of polyamide nanofiltration membranes via dragging piperazines to enhance ion selectivity. *J. Membr. Sci.* **2023**, *667*, 121187.

(10) Han, S.; Mai, Z.; Wang, Z.; Zhang, X.; Zhu, J.; Shen, J.; Wang, J.; Wang, Y.; Zhang, Y. Covalent Organic Framework-Mediated Thin-Film Composite Polyamide Membranes toward Precise Ion Sieving. *ACS Appl. Mater. Interfaces* **2022**, *14* (2), 3427-3436.